

Interannual Variations of Volume Transport in the Western Labrador Sea Based on TOPEX/Poseidon and WOCE Data

GUOQI HAN AND C. L. TANG

Coastal Ocean Sciences, Fisheries and Oceans Canada, Bedford Institute of Oceanography, Dartmouth, Nova Scotia, Canada

(Manuscript received 1 December 1999, in final form 31 March 2000)

ABSTRACT

The interannual variations of volume transport in the western Labrador Sea are estimated using six years of TOPEX/Poseidon altimeter data and hydrographic data from a WOCE repeat section and a method based on the linear momentum equation in which the sea surface is the level of known motion. The interannual variation of the total transport in spring/summer has a range of 6.2 Sv ($\text{Sv} \equiv 10^6 \text{ m}^3 \text{ s}^{-1}$) and is positively correlated with the fall/winter North Atlantic Oscillation (NAO) index and wind patterns in the northwest North Atlantic. The total transport anomaly is decomposed into a barotropic and a baroclinic component. The interannual change of the barotropic transport is similar to that of the total transport, and is positively correlated with the fall/winter NAO index. The baroclinic transport anomaly, in comparison, has a smaller magnitude and the opposite sign. The authors conjecture that the deepened Icelandic low in high index years generates a strong cyclonic wind stress curl, which in turn creates a strong divergence and a large upward sea surface slope toward the Greenland coast, resulting in an intensified Labrador Sea circulation.

1. Introduction

The circulation of the Labrador Sea (Fig. 1) has been studied over the last 30 years using hydrographic data, current meter data, drifters, ice beacons, and numerical models (e.g., Lazier 1973; LeBlond et al. 1981; Lazier and Wright 1993; Tang et al. 1996). These studies have confirmed the finding of an early Coast Guard survey (Smith et al. 1937) that the mean basin-scale circulation is cyclonic and show that the circulation variability can be caused by local air–sea fluxes, boundary forcing, and other factors. On the northern boundary, the inflow and outflow through Davis Strait connect the waters of the Labrador Sea and Baffin Bay. South of Greenland, the East Greenland Current along the shelf edge, Irminger Current over the continental slope, and the Denmark Strait Overflow near the bottom of the deep sea, provide the bulk of the volume transport into the Labrador Sea. In addition to fluctuations of inflows at the lateral boundaries atmospheric fluxes, river runoff, and ice formation/melt can also change the water properties and hence the circulation. Persistent atmospheric cooling in an extremely cold winter can cause deep convection and occurrence of a cyclonic gyre in

the western Labrador Sea (Clarke and Gascard 1983). The fluctuations of the atmospheric forcing over the North Atlantic (Deser and Blackmon 1993) are expected to have significant impacts on the circulation of the Labrador Sea.

There have been a number of studies of the seasonal and interannual variabilities of the Labrador Sea circulation. Thompson et al. (1986) employed the topographic Sverdrup relationship to calculate the seasonal transport, and obtained a seasonal range of 7 Sv ($\text{Sv} \equiv 10^6 \text{ m}^3 \text{ s}^{-1}$). They found the topographic Sverdrup transport is mainly over the deep continental slope. From the results of a wind-driven barotropic model of the North Atlantic, Greatbatch and Goulding (1989) found that Labrador Sea transport increased by ~ 5 Sv between July and January. Myers et al. (1989) estimated the interannual variability of the geostrophic transport in the upper 100 m of the Labrador and Newfoundland shelves from historical hydrographic data and found a weak negative correlation between the southward transport and the winter North Atlantic Oscillation (NAO) index. An analysis of current-meter and density data by Lazier and Wright (1993) estimated an annual transport of 4 Sv shoreward of the 1400-m isobath at the Hamilton Bank section.

With the advent of precise satellite altimetry in the 1990s, the study of the Labrador Sea transport entered a new phase. Using the TOPEX/Poseidon (T/P) and Geosat altimeter data, Han and Ikeda (1996) investi-

Corresponding author address: Dr. Guoqi Han, Coastal Ocean Science, Bedford Institute of Oceanography, Post Office Box 1006, Dartmouth, Nova Scotia B2Y 4A2, Canada.
E-mail: ghan@emerald.bio.dfo.ca

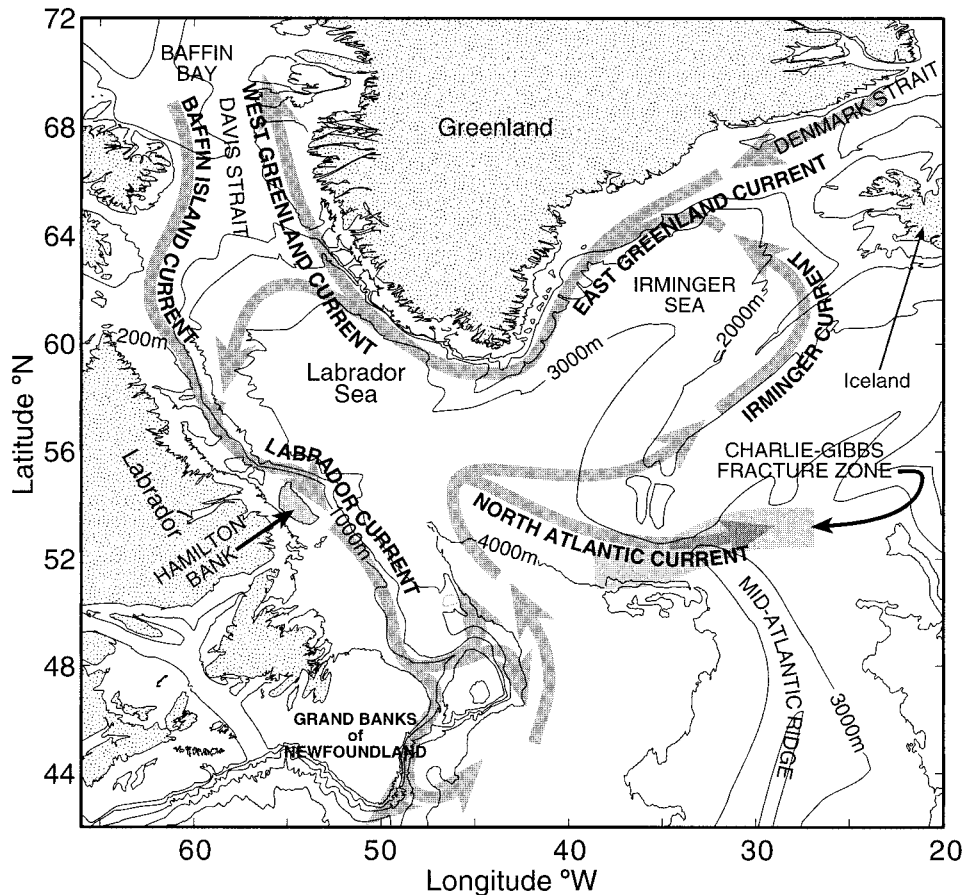


FIG. 1. Diagram showing the Labrador Sea, its environs and major currents, modified from Lazier and Wright (1993). The 2000- and 3000-m isobaths east of 40°W are heavily smoothed for clarity.

gated the annual variability of sea surface topography. Their results indicated the predominance of the steric height effect over the wind-driven barotropic response. Recently, Han and Tang (1999) used T/P altimeter data from late 1992 to early 1996, concurrent winds, and historical hydrographic data to study the seasonal variations of velocity and transport in the Labrador Current. They presented a method to calculate currents and transports from altimeter and density data using the sea surface as the level of known motion, and found a range of 10 Sv in the seasonal transport at the Hamilton section. The transport was largest in winter and smallest in spring, consistent with moored measurements in Lazier and Wright (1993).

In this study, we compute the volume transport of the Labrador Sea circulation from six years of T/P altimeter data along two ascending tracks and density data from a repeat World Ocean Circulation Experiment (WOCE) hydrographic section across the Labrador Sea (Fig. 2). The computation uses the sea surface as the level of known motion inferred from the altimeter data, without the uncertainty of the traditional geostrophic calculation due to an assumed level of no motion. The purpose is

to obtain an estimation of the interannual variability of the volume transport from the data, and the barotropic and baroclinic contributions to the transport variability. We also seek possible correlation between the Labrador Sea circulation and atmospheric forcing, both local and large scale.

The paper consists of six sections. Section 2 describes the data processing techniques. The transport calculations and error estimations are given in section 3. Section 4 presents the results for volume transport, the barotropic and baroclinic contributions. Correlation between the NAO and the Labrador Sea circulation is identified and possible causes for the variations of transport are discussed in section 5. Section 6 summarizes the findings of the study.

2. Data

a. T/P altimeter data

We use 1-s altimeter data from October 1992 to September 1998, with an alongtrack ground resolution of 5.9 km. The data were obtained from the NASA Path-

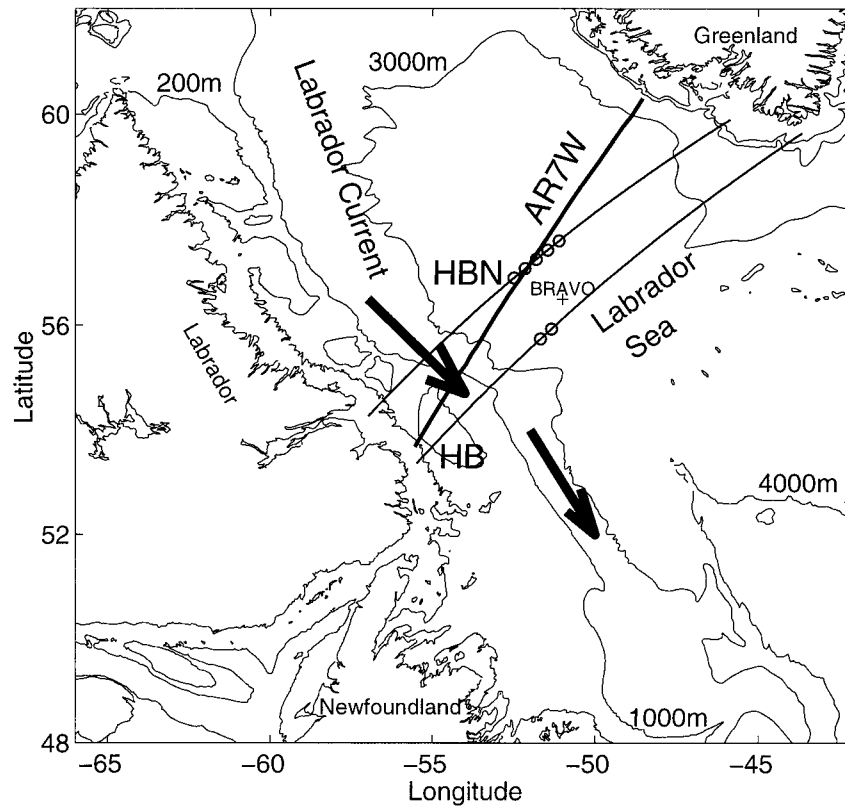


FIG. 2. Map showing the study area: **HB** and **HBN** are two TOPEX/Poseidon ascending ground tracks that straddle the AR7W hydrographic section in the western Labrador Sea. The 200-m, 1000-m, 3000-m, and 4000-m isobaths (thin lines) and the location of the Labrador Current (thick arrows) are also shown. The five open circles on **HBN** indicate the outer limits of integration in the calculation of the volume transport, from the deepest sea westward at an interval of 25 km. The corresponding outer limits for **HB** (for clarity only the easternmost and westernmost locations are shown) are determined from the values of H/f .

finder Project and Jet Propulsion Laboratory. The T/P satellite repeats its ground track every 9.9156 days, thus giving about 216 observations during our study period at each location under ideal conditions. However, the actual number of data points over the Labrador Shelf is smaller because of ice cover during winter and early spring.

The data were edited using quality flags and parameter ranges recommended by JPL (Benada 1997). Corrections were made to account for various instrumental, atmospheric, and some oceanographic effects. The atmospheric corrections include the ionospheric delay and the wet and dry tropospheric delays. The sea state bias, the inverse barometric response of the sea surface to the atmospheric pressure change, and the elastic ocean, solid earth, and pole tides were among the oceanographic corrections. The Goddard Space Flight Center precise orbit based on the joint gravity model-3 (JGM-3) was used.

Accuracy of the altimetric sea surface height data depends on that of the altimeter range measurement and its corrections, the reference ocean geoid, and the

satellite orbit. Since the ocean geoid is time invariant, we separated time-varying height anomalies from mean heights calculated for the study period. The mean sea surface heights were computed only at locations where more than 100 observations of the corrected sea surface height data were available. The sea surface height anomalies were then calculated by removing the means. The dataset for the altimetric height anomalies was divided into four seasons each year: winter (Jan–Mar), spring (Apr–Jun), summer (Jul–Sep), and fall (Oct–Dec), resulting in 24 height anomalies at each location, which are independent of the geoid and its associated errors.

We selected two ascending T/P ground tracks (Fig. 2) that partially overlap the conductivity-temperature-depth (CTD) section for detailed analysis. Prior to seasonal averaging, the data were smoothed along the satellite track and in time using Gaussian filters with e -folding scales of 25 km and one month to remove the short wavelength variability and random noise. Figure 3 shows examples of the smoothed data (fall and summer). The total range of sea level variability (seasonal and

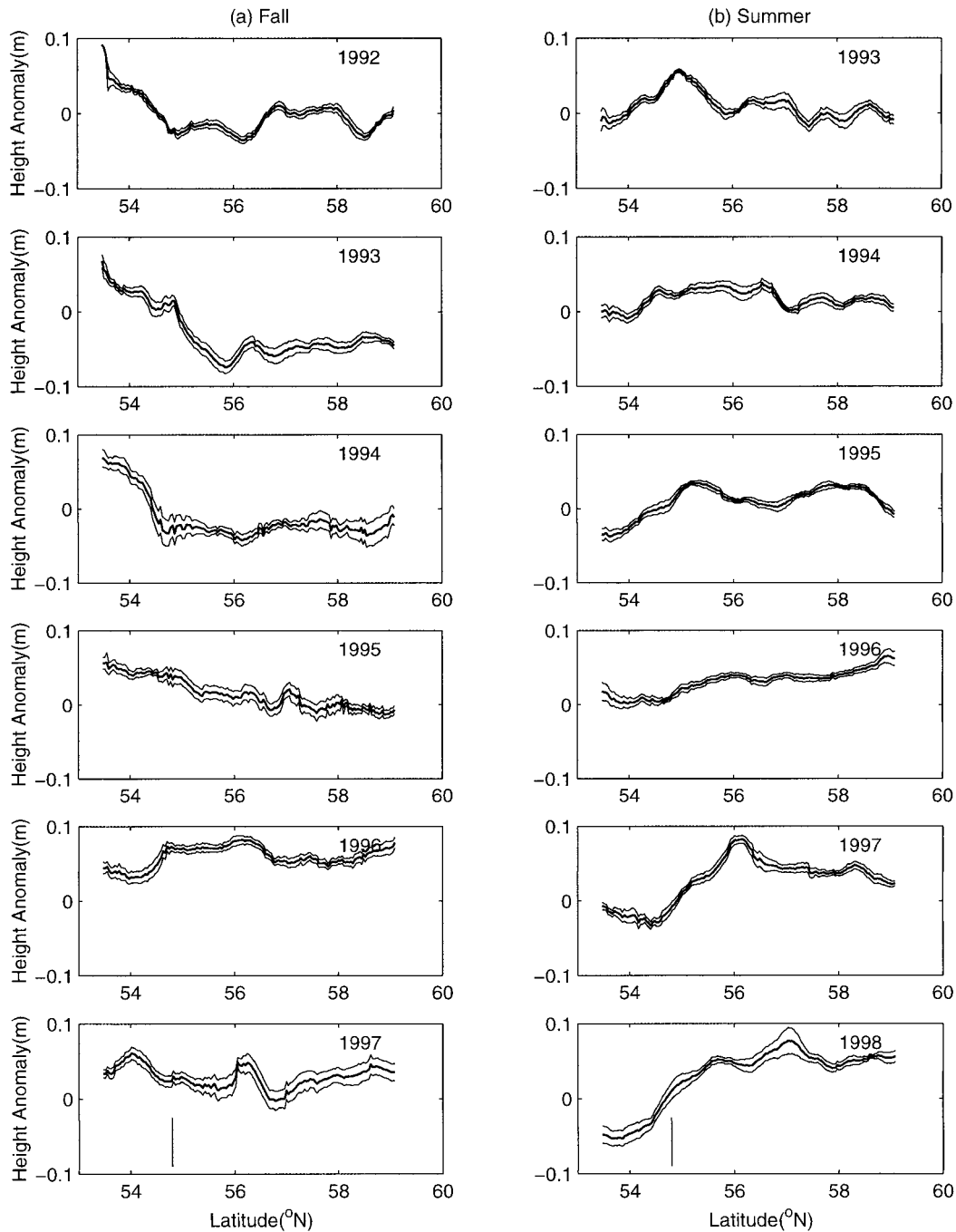


FIG. 3. Seasonal sea surface height anomalies (thick curves) from TOPEX/Poseidon data and associated standard errors (thin curves) on **HB** in (a) fall and (b) summer from 1992 to 1998. The vertical line in the two lowest panels indicates the location of the 1000-m isobath over the Labrador continental slope.

interannual) is of the order 0.15 m and the standard errors are typically ~ 0.01 m. The seasonal difference of the order 0.1 m is evident. The sea level tilts upward in fall and downward in summer against the Labrador coast, indicating a larger southward transport in fall (Han and Tang 1999).

b. Hydrographic data

Density profiles used for this study were computed from CTD data on the AR7W section across the Labrador Sea (Fig. 2). The AR7W section has been occupied by the Bedford Institute of Oceanography every summer

TABLE 1. Information about the density data on the AR7W CTD section used in this study: date of the CTD occupation and number of stations from 1993 to 1998.

| Year | Date | No. of stations |
|------|--------------|-----------------|
| 1993 | 19–23 Jun | 26 |
| 1994 | 28 May–5 Jun | 29 |
| 1995 | 11–16 Jun | 30 |
| 1996 | 18–25 May | 29 |
| 1997 | 21–28 May | 23 |
| 1998 | 26 Jun–3 Jul | 23 |

since 1990, as one of Canada’s contributions to the WOCE. Table 1 gives relevant information about this section for the years used in this study. The CTD data were calibrated and subsampled to 9-m depth intervals (I. Yashayaev 1999, personal communication). All the calculations involving density in the paper are based on the subsampled dataset.

The density sections for 1994 and 1996 (Fig. 4) clearly show the large horizontal density gradients over the shelf break and upper slope where the traditional Labrador Current is located. The gradients decrease rapidly toward the shore and the deep water. Comparing the density distribution in 1994 with that in 1996, we can see more Labrador Sea Water with potential density between 27.76 and 27.78 kg m⁻³ in 1994 due to convective overturning. The isopycnals associated with northwest Atlantic deep water (potential density between 27.80 and 27.88 kg m⁻³) in 1994 have much larger negative slopes seaward in the western Labrador Sea than in 1996, implying substantial differences in the magnitude

of the associated geostrophic transport. The Denmark Strait Overflow water in the deepest layer is much thinner in 1994 than in 1996.

3. Analysis method

a. Volume transport calculation

In this section, we outline the method to compute the depth-averaged velocity and transport from the altimetric and hydrographic data. The computation is based on the time-independent momentum equation with the nonlinear and horizontal friction terms neglected. The equation for velocity v , perpendicular to a vertical transect, is given by

$$-fv = -\frac{1}{\rho_0} \frac{\partial p}{\partial x} + \frac{1}{\rho_0} \frac{\partial \tau}{\partial z} \tag{1}$$

$$p = g\rho_0\zeta + g \int_z^0 \rho dz, \tag{2}$$

where v is positive northward; x is the horizontal coordinate along the transect with $x = 0$ at the Labrador coast increasing offshore; f is the Coriolis parameter; p is the pressure; z is the vertical coordinate positive upward with $z = 0$ at the mean sea level; g is the gravity acceleration; ρ is the density of water; ρ_0 is the reference density; τ is the x component of the shear stress, which has a significant magnitude only in the surface and bottom boundary layer; and ζ is the sea surface height

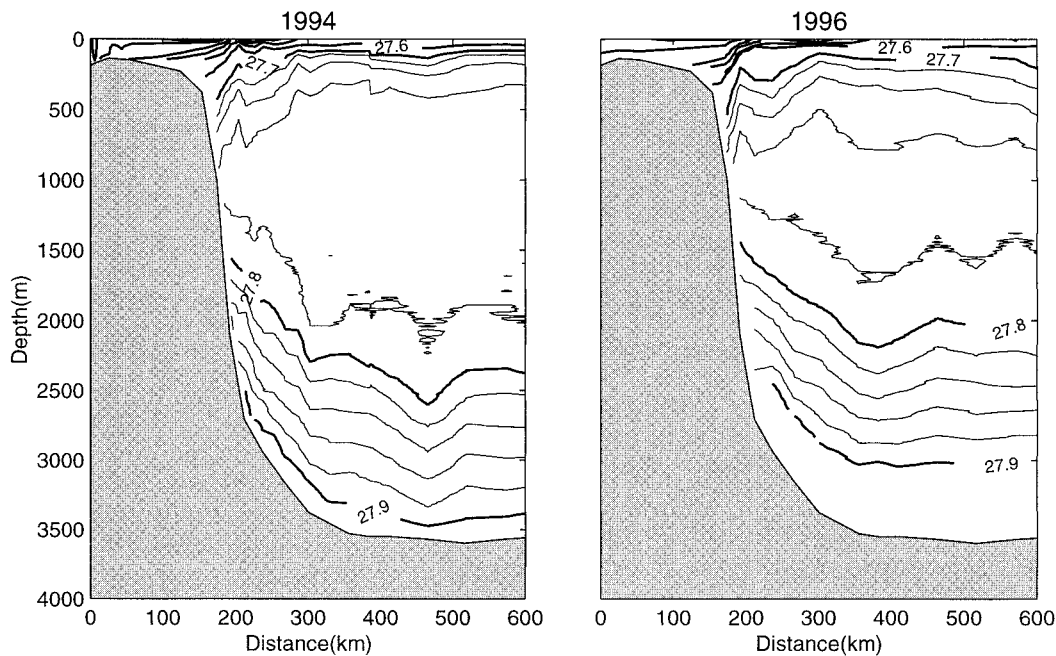


FIG. 4. Potential density (kg m⁻³) distribution across the AR7W CTD section in early summer for 1994 and 1996. The thick-contour intervals are 0.5 kg m⁻³ for density below 27.0 kg m⁻³, 0.1 kg m⁻³ for density above 27.6 kg m⁻³, and 0.2 kg m⁻³ otherwise. The thin-contour interval is 0.02 kg m⁻³ for density between 27.7 and 27.9 kg m⁻³.

referenced to an ocean geoid, adjusted for the effect of the local atmospheric pressure.

The geostrophic current at z relative to a reference depth z_0 , $v_G(z, z_0)$, is given by

$$v_G(z, z_0) = -\frac{g}{\rho_0 f} \int_{z_0}^z \frac{\partial \rho}{\partial x} dz. \quad (3)$$

The bottom current is defined as the current just above the bottom boundary layer and is assumed to be in geostrophic balance. This current is related to the sea surface slope and the surface geostrophic current relative to the bottom by

$$v(-H) = \frac{g}{f} \frac{\partial \zeta}{\partial x} - v_G(0, -H), \quad (4)$$

where H is the local water depth.

In the absence of wind stress, the surface current is determined solely by sea surface slope. Neglecting the shear stress term in (1), we have

$$v(0) = \frac{g}{f} \frac{\partial \zeta}{\partial x}. \quad (5)$$

Integrating Eq. (1) over the depth and neglecting the bottom Ekman layer, we have the depth-averaged velocity normal to the transect, V :

$$V = \frac{g}{f} \frac{\partial \zeta}{\partial x} + \frac{1}{f} \int_{-H}^0 \frac{\partial b}{\partial x} dz + \frac{1}{Hf} \int_{-H}^0 z \frac{\partial b}{\partial x} dz - \frac{1}{\rho_0 f H} \tau_0 \quad (6)$$

$$b = \frac{g}{\rho_0} [\rho(x, z) - \bar{\rho}(z)], \quad (7)$$

where b is the buoyancy parameter, τ_0 is the along-transect component of surface wind stress, and $\bar{\rho}(z)$ is a reference density obtained by averaging ρ at a given depth across the transect. The four terms on the right-hand side of Eq. (6) correspond to the contributions from sea surface slope (first term), density (second and third terms), and local wind stress (fourth term), respectively. From Eq. (2) and (3), we can see that the sum of the first two terms of Eq. (6) is equal to the geostrophic bottom current.

Following Fofonoff (1962), we define the transport due to the bottom current as the barotropic transport, T_B :

$$T_B \equiv H v(-H) = \frac{g}{f} H \frac{\partial \zeta}{\partial x} + \frac{H}{f} \int_{-H}^0 \frac{\partial b}{\partial x} dz. \quad (8)$$

The contribution of the geostrophic currents relative to the bottom current, $v_G(z, -H)$, to the total transport is defined as the baroclinic transport:

$$T_G \equiv \int_{-H}^0 v_G(z, -H) dz = \frac{1}{f} \int_{-H}^0 z \frac{\partial b}{\partial x} dz. \quad (9)$$

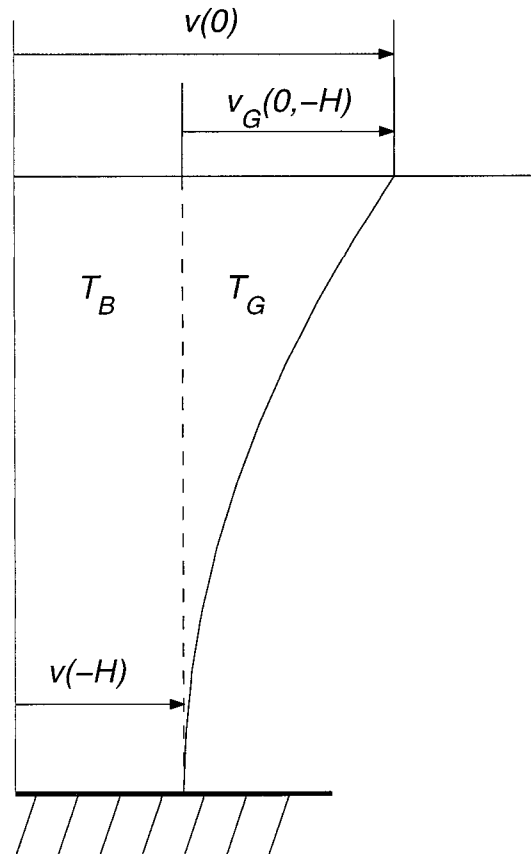


FIG. 5. Diagram for the definition of the current components and transports.

This is simply the third term of Eq. (6) multiplied by H . The relationship among the barotropic and baroclinic transports, surface currents, and bottom current is illustrated in Fig. 5.

The total transport is the sum of the barotropic, the baroclinic, and the Ekman transports:

$$T = T_B + T_G - \frac{\tau_0}{\rho_0 f}. \quad (10)$$

For currents on seasonal and interannual timescales, the Ekman transport is very small compared to T_B and T_G . An order of magnitude estimate of the Ekman transport using a mean wind speed of 6 m s^{-1} and a water depth of 300 m in Eq. (6) gives a depth-averaged current of 0.0018 m s^{-1} . This is two orders of magnitude smaller than a typical current on the shelf and can be neglected (Han and Tang 1999). We will therefore neglect the Ekman transport contribution to the volume transport in all following calculations and discussions.

Another widely used definition of current components is that the barotropic current is the vertically averaged current and the baroclinic current is the difference between the total current and the barotropic current. By this definition, the barotropic transport is the total transport in Fofonoff's definition and is related to the sea

surface slope through the continuity equation. Although in Fofonoff's definition, density appears in both the barotropic and baroclinic currents, Eq. (9) is consistent with the conventional definition of geostrophic transport. If the level of no motion in the calculation is set to the sea bottom, T_G is equal to the geostrophic transport (i.e., the barotropic transport vanishes). The cumulative volume transport across a section can be calculated by integrating T from x_1 to x_2

$$\int_{x_1}^{x_2} (T_B + T_G) dx = \text{BT} + \text{BC}, \quad (11)$$

where BT and BC are the cumulative barotropic and baroclinic transports, respectively, given by

$$\text{BT} = \frac{g}{f} \int_{x_1}^{x_2} \frac{\partial \zeta}{\partial x} H dx + \frac{1}{f} \int_{x_1}^{x_2} H \int_{-H}^0 \frac{\partial b}{\partial x} dz dx \quad (12)$$

$$\text{BC} = \frac{1}{f} \int_{x_1}^{x_2} \int_{-H}^0 z \frac{\partial b}{\partial x} dz dx. \quad (13)$$

Computation of the derivative of discrete data is notoriously sensitive to how the data are filtered. However, if the derivative is inside an integral, we can bypass this problem by using integration by parts. Equations (12) and (13) can be transformed into the following forms:

$$\text{BT} = \frac{g}{f} \left[(\zeta H)_2 - (\zeta H)_1 - \int_{x_1}^{x_2} \frac{\partial H}{\partial x} \zeta dx + (\phi H)_2 - (\phi H)_1 - \int_{x_1}^{x_2} \frac{\partial H}{\partial x} \phi dx - \frac{1}{g} \int_{x_1}^{x_2} \frac{\partial H}{\partial x} H b_H dx \right] \quad (14)$$

$$\text{BC} = \frac{g}{f} \left[(\eta)_2 - (\eta)_1 + \frac{1}{g} \int_{x_1}^{x_2} \frac{\partial H}{\partial x} H b_H dx \right], \quad (15)$$

where

$$\phi = \frac{1}{g} \int_{-H}^0 b dz, \quad \eta = \frac{1}{g} \int_{-H}^0 b z dz,$$

and b_H is the buoyancy parameter at the sea bottom.

In Eqs. (14) and (15), only the sea surface height is required, while in Eqs. (12) and (13) the sea surface slope must be calculated first.

b. Error estimation

We estimated the errors in the cumulative barotropic and baroclinic transports from Eqs. (14) and (15) assuming that there is no error in the water depth H . The resultant error is defined as the root sum square of the errors of the individual terms in each equation. For the terms involving altimeter data, the standard errors of the seasonal-mean sea surface height anomalies were calculated (Fig. 3). Typical errors in the cumulative barotropic transport from the outer Labrador Shelf to the 3600-m isobath associated with the altimeter data are estimated at ~ 2 Sv from Eq. (14).

For the terms involving density, errors from two sources are considered here. One is measurement error, and the other is statistical error arising from our use of the instantaneous density as proxy for the seasonal-mean density. The measurement error is negligible compared to the statistical error. For the statistical error, we made use of the abundant historical data available at the Ocean Weather Station (OWS) Bravo (56.5°N, 51°W) as representative of the entire section since data in other parts of the deep Labrador Sea are scarce. The density errors

(defined as the standard deviations from the seasonal means) in spring and summer were calculated year by year from the historical data and then averaged over the years. The averaged errors decrease rapidly from the surface to the deep water and become negligibly small at 1500 m. The errors of ϕ and η were obtained by vertically integrating the averaged errors from the surface to the 1500-m depth and then used in Eqs. (14) and (15) to compute the errors in BT and BC. From the outer Labrador Shelf to the 3600-m isobath, the errors in BT and BC associated with the density data were estimated at 2.5 and 0.3 Sv, respectively.

4. Interannual variability of volume transport

The total cumulative volume transport can be calculated from Eqs. (14) and (15) if concurrent altimetric and hydrographic data are available. Due to the limited availability of the CTD data (see Table 1), we used the instantaneous CTD data as proxy for the seasonal means. The error due to such an approximation is discussed in section 3. In computing the terms in Eqs. (14) and (15) involving sea level, we used the spring and summer T/P data for each year. The spring and summer transports were then averaged to obtain a mean transport representing the mean transport from April to September. The choice of the averaging period is primarily dictated by the availability of the data and the size of the errors.

The WOCE AR7W section lies between **HB** and **HBN** in the western Labrador Sea. In computing the terms involving sea surface height in Eqs. (14) and (15), we

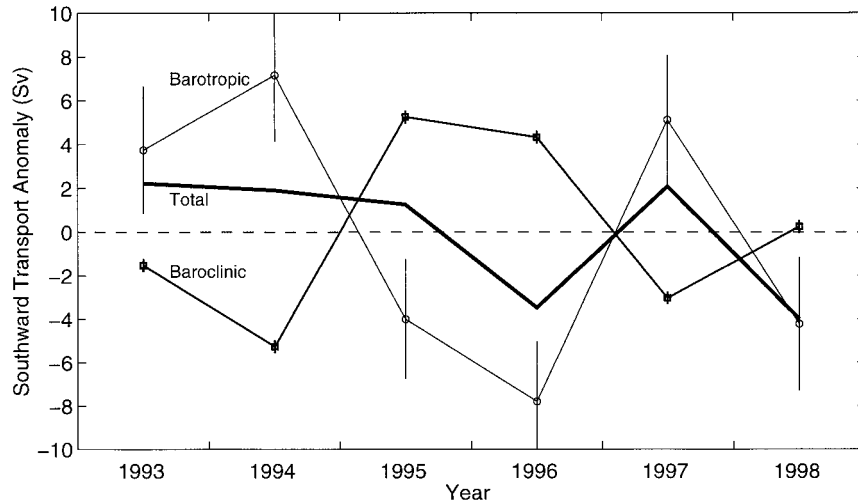


FIG. 6. Cumulative southward transport anomaly in the western Labrador Sea (west of the open circles in Fig. 2) as a function of year. The total transport (thick lines) is the sum of barotropic (circles) and baroclinic (squares) components. The standard errors are shown as vertical lines. The errors associated with the barotropic component are calculated as the root sum square of the errors in both the altimetric sea surface height anomaly and in ϕ . The errors associated with baroclinic component are calculated from the error in η . The errors associated with the total transport are not shown in the figure for graphic clarity.

averaged the results computed separately for the two tracks. The outer limits of the integration were points on the two tracks with the same values of H/f . This was based on the assumption that currents flowed along the H/f contours. The distance between **HB** and **HBN** is approximately 100 km. Five points on **HBN** with a spatial interval of 25 km and their corresponding points on **HB** were used as the outer limits of the integration (see Fig. 2 for locations of the outer limits). The transports from a common westernmost point (approximately located at the Labrador shelf break) to the five outer points were then averaged, to reduce the sensitivity of the results to currents with a spatial scale of less than 100 km. Note that the easternmost point on **HB** is located at the maximum water depth.

Figure 6 shows the averaged southward transport anomalies from 1993 to 1998. In the plot, a positive anomaly corresponds to a larger than average southward transport. The range of the total cumulative transport variation is about 6.2 Sv. The years 1993, 94, 95, and 1997 have larger than average transports, and 1996 and 1998 have smaller than average transports. The variation of the barotropic transport follows that of the total transport. The baroclinic transport, by comparison, is smaller in magnitude and has opposite sign. The barotropic and baroclinic components compensate each other, resulting in a total transport anomaly smaller than the barotropic transport anomaly.

The error in the baroclinic component is insignificant compared to the total transport, but the mean error in the barotropic component, ± 2.8 Sv, is large. The large error is inevitable owing to the small number of data points from T/P in a given season of a year. Despite the

size of the error, the range over the 6-yr period is much greater than the error. The error associated with the total transport may be calculated as the root-sum-square of the errors in the barotropic and baroclinic transports, and so is approximately the same as the error in the barotropic transport.

5. Discussion

The interannual variations in the volume transport can be caused by many factors, both oceanographic and atmospheric. The Labrador Sea circulation is a part of the North Atlantic circulation, the variability of which is believed to be a consequence of global air–ice–ocean interactions. Any change in the water properties and circulation in the North Atlantic can have discernable signals in the Labrador Sea.

In an attempt to provide an explanation for the results presented in the previous section, we search for possible links between the Labrador Sea and the atmospheric conditions, both local and large scale. We start with the large-scale atmospheric forcing in the North Atlantic. An intuitive view of the large-scale winter atmospheric conditions of the North Atlantic is shown in Fig. 7. From 1993 to 1995, the Icelandic Low lies 500-km southwest of Iceland with a sea level pressure of 991–993 mb at the low-pressure center. Strong winds appear south of Greenland and east of Newfoundland. In 1996 there is a dramatic change of the pattern. The low-pressure area has extended to the central and northern Labrador Sea and the minimum pressure rises to 1003 mb with an associated weak wind field. The atmospheric patterns

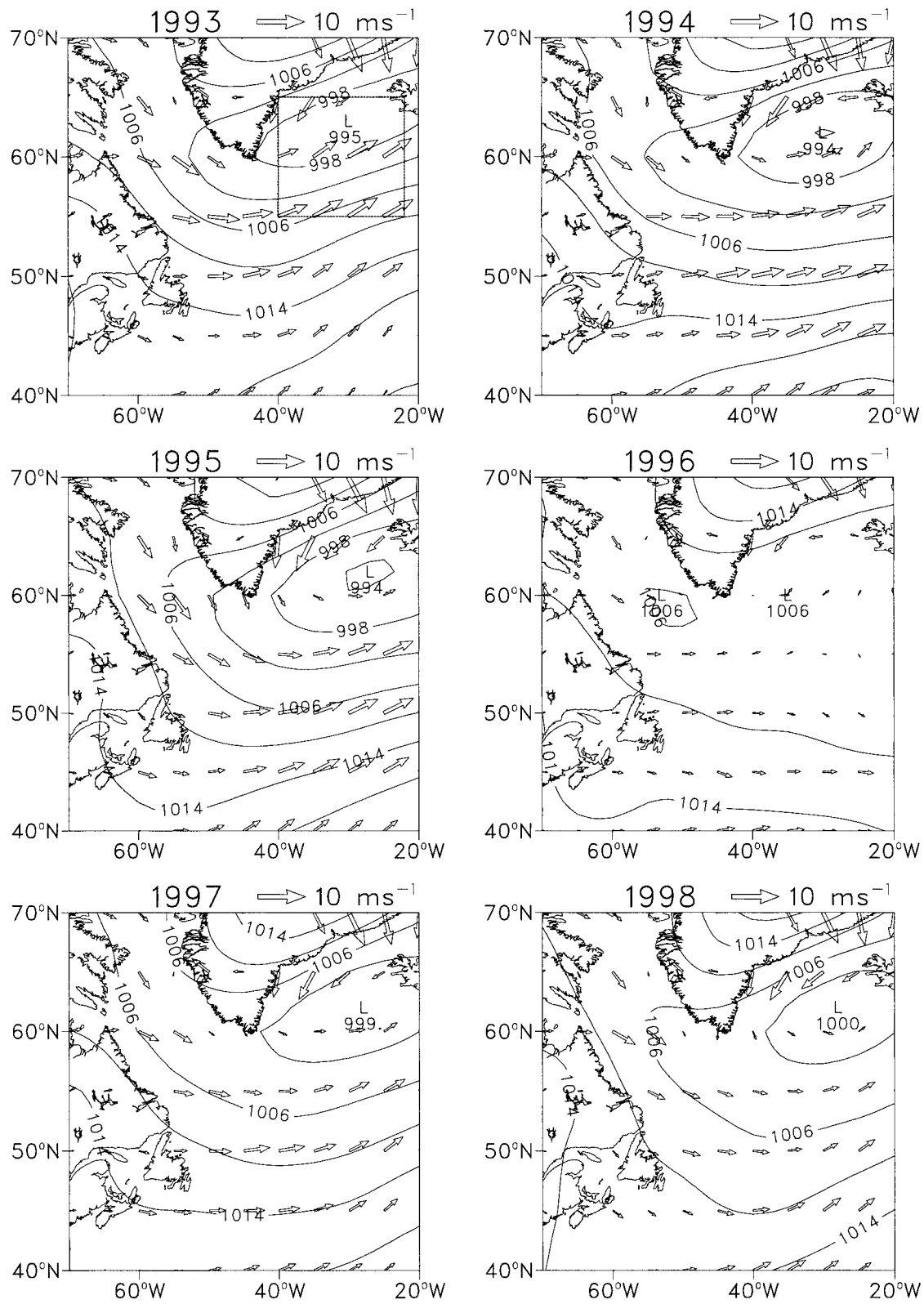


FIG. 7. Sea level pressure (mb) and 10-m wind velocity vectors in winter from the NCEP-NCAR reanalysis. The enclosed box southeast of Greenland in the upper-left panel indicates the region over which the mean wind stress curl in Fig. 8c is calculated.

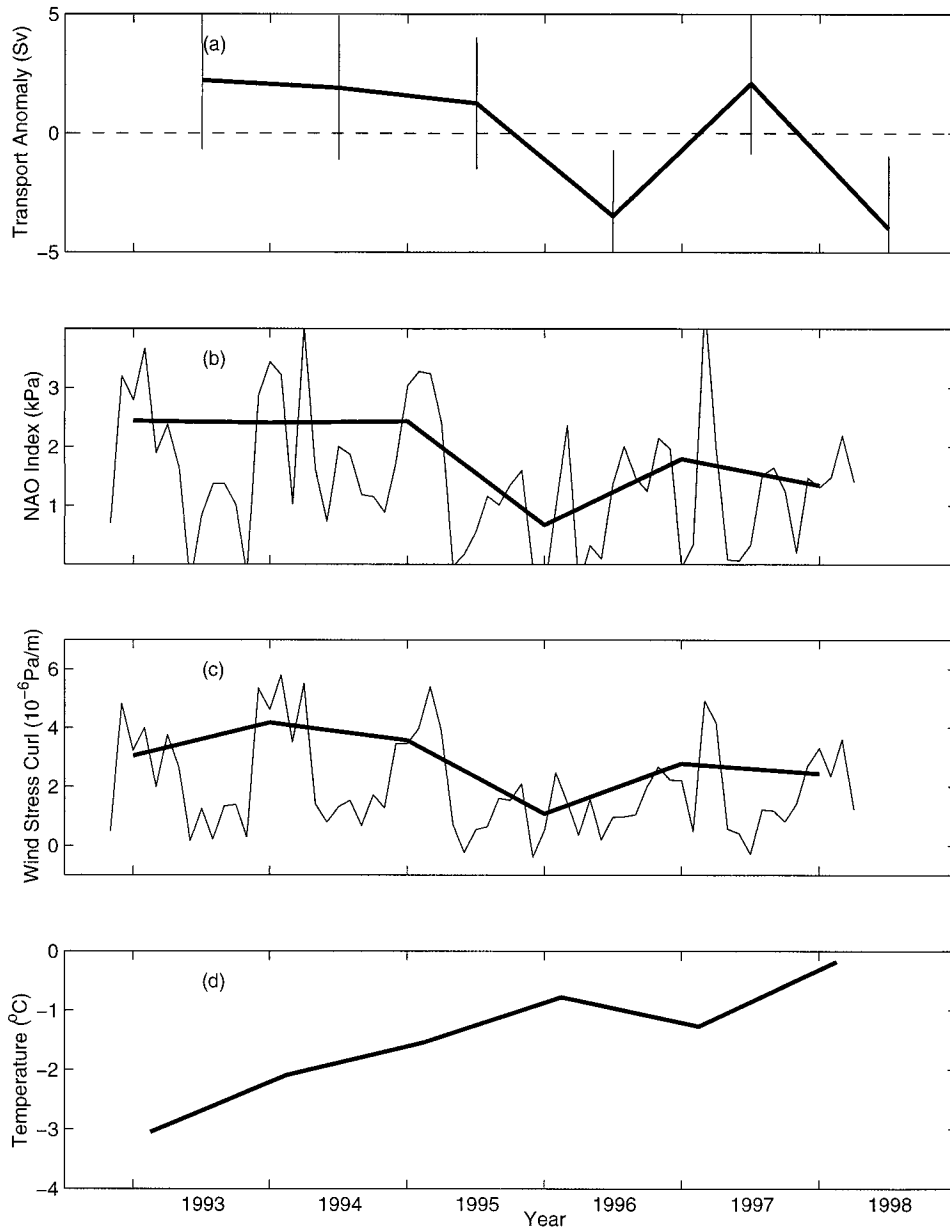


FIG. 8. (a) Total southward transport anomalies in spring/summer, (b) anomalies of fall/winter NAO indices defined as the sea level pressure difference between the Azores high and the Icelandic low, (c) mean fall/winter wind stress curl in a region southeast of Greenland (see Fig. 7), and (d) winter sea level air temperature at OWS Bravo. The vertical lines in (a) indicate standard errors of transport. In (b) and (c), the thin lines are the monthly values and the thick lines are Oct–Mar average. The data are from the NCEP–NCAR reanalysis.

in 1997 are similar to those from 1993 to 1995, while the patterns in 1998 are similar to those in 1996.

An indicator of the dominant mode of atmospheric variability in the North Atlantic is the NAO index, which is conventionally defined as the difference in sea level pressure between the Azores and Iceland. A large positive index is usually associated with strong westerlies and a deepened Icelandic low. The NAO index has been used by several investigators to explain the

interannual variability of sea ice and other variables in the Labrador Sea (Colbourne et al. 1994; Drinkwater 1996; Mysak et al. 1996). Figure 8b shows the monthly NAO indices and the fall/winter (Oct–Mar) means from the NCEP–NCAR reanalysis data (Kalnay et al. 1996; DeTracey and Tang 1997). The fall/winter NAO indices show a significant interannual variation, high in 1993–95 and 1997 and low in 1996 and 1998.

Wind stress curl associated with the Icelandic low can

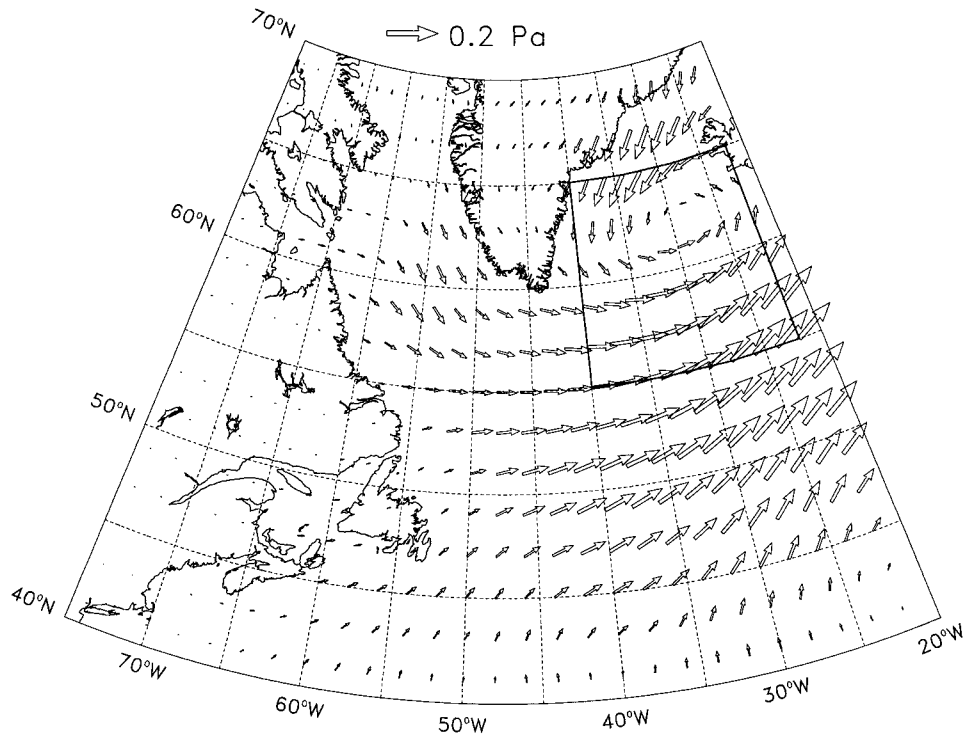


FIG. 9. Differences between the fall/winter wind stress in 1994 and that in 1996. The wind stress was computed from the NCEP–NCAR reanalysis dataset. The region over which the mean wind stress curl in Fig. 8c is calculated is also indicated.

provide boundary forcing for the Labrador Sea circulation. We calculated the wind stress curl by performing a line integration of monthly wind stress around the perimeter of a box enclosing the low pressure center (see Fig. 7 for location of the box). The integrated wind stress divided by the area of the box represents the mean wind stress curl over the box. The monthly wind stress was calculated from 6-hourly vector winds using a bulk formula averaged over a month. The monthly time series and the October–March average of the mean wind stress curl (Fig. 8c) show that there are significant seasonal and interannual variations. Strong wind stress curl occurs in the fall and winter of 1993/94, 1994/95, 1995/96, 1997/98.

Within the Labrador Sea air temperature, precipitation, and wind are major factors determining the heat and water fluxes, which can impact the water properties directly and the current and transport indirectly (Tang et al. 1999). Figure 8d is the winter air temperature at OWS Bravo computed from the NCEP–NCAR data, which shows a significant interannual variation. The air temperature in the winter of 1993 and 1994 is lower, by about 2°C than that in the winter of 1996 and 1998. Note that the NAO may have a significant impact on the local atmospheric conditions in the Labrador Sea and thus the local air temperature may not be considered an independent factor affecting the transport variability.

The change of the total southward volume transport

in spring/summer (Fig. 8a) seems to be positively correlated with the NAO index (Fig. 8b) and wind stress curl associated with the Icelandic low (Fig. 8c) in the preceding fall/winter. The transport variability also appears to be negatively correlated with the winter surface air temperature (Fig. 8d). The high NAO index and high wind stress curl years of 1993, 94, 95, and 97 all have corresponding above average southward transports, and the opposite is true for 1996 and 1998 (Fig. 8). The relationship of the Labrador Sea circulation with the wind stress field associated with the Icelandic low is further indicated from the wind stress difference between 1994 (a year with high NAO index) and 1996 (a year with low NAO index) (Fig. 9). Over the northwestern North Atlantic, the strongest wind stress curl difference occurs in the area southeast of Greenland. A calculation for the Labrador Sea similar to that in Fig. 8c indicates that the magnitude of the wind stress curl over the Labrador Sea (not shown) is less than half of that over the Icelandic low. There is no obvious correlation between the Labrador Sea wind stress curl and the Labrador Sea transport. This implies that the local wind stress curl does not play an important role in the interannual variation of the transport in the Labrador Sea. We conjecture that the interannual variability of the Labrador Sea gyre transport is a remote response to change in the NAO. The deepened Icelandic low in the years with high NAO index generates a strong cyclonic

wind stress curl southeast of Greenland (Figs. 8c and 9), which creates a strong divergence and large upward sea surface slope toward the southeast Greenland coast. The increased sea surface slope enhances southwestward geostrophic flow off southeast Greenland, which then intensifies the Labrador Sea circulation through large-scale advection. The effect can last into the spring/summer months because change in sea surface slope by seasonal-scale wind stress curl is determined by the time history of the wind field (quasigeostrophic motion). This may explain the correspondence between the fall/winter NAO index and the total volume transport in spring/summer. The year 1995 has a high fall/winter index but very low spring/summer index, which may be the reason for the relatively low total transport in 1995.

The interannual variation of the baroclinic transport is opposite to that of both the total and barotropic transports (Fig. 6), that is, negatively correlated with the NAO index. This negative correlation with the NAO index is consistent with Myers et al.'s (1989) finding for the summer baroclinic transport relative to 100 m. They suggest that following winters of strong westerlies, the shelf-break density front is weaker in summer. The baroclinic transport in this study was computed relative to the sea bottom. Its interannual variation appears to be associated with significant changes of density gradient at depth over the lower continental slope (Fig. 4). The negative correlation with the NAO index suggests that the horizontal distribution of density in the western Labrador Sea could be related to the large-scale atmospheric forcing through large-scale ocean circulation and/or convective overturning.

The range of the interannual transport variability, 6.2 Sv, is a significant fraction of the absolute gyre transport, and is comparable to the calculated seasonal variability of 10 Sv (Han and Tang 1999). The absolute transport was estimated at 35–50 Sv based on ship data, ice beacon data, and model results (Clarke 1984; Reynaud et al. 1995; Tang et al. 1996). The absolute transport has also been computed from T/P data and two geoids, OSU91A (Rapp et al. 1991) and GSD95 (Veronneau 1995), by Han and Tang (1998). They obtained a value of 50 Sv.

6. Conclusions

We have made a quantitative estimation of the interannual variability of the volume transport in the western Labrador Sea using T/P satellite altimeter data, and WOCE data taken from 1993 to 1998. The combined use of the two data sources allows a unique determination of the volume transport without making a priori assumption of the level of no motion.

The interannual range of the transport of the Labrador Sea gyre is about 6.2 Sv, which is comparable to its seasonal range of 10 Sv, and represents a significant fraction of the estimated mean transport of 35–50 Sv. The transport was above average in 1993 to 1995 and

in 1997, and below average in 1996 and 1998. The variability of the total volume transport in the Labrador Sea circulation is positively correlated with the winter NAO index. The baroclinic transport component is smaller than the barotropic transport component in magnitude, and the two components are opposite in sign. The large-scale wind field over the northwestern North Atlantic seems to be the dominant factor for the interannual change of the volume transport in the Labrador Sea.

Acknowledgments. We thank Igor Yashayaev for providing the calibrated CTD data from the WOCE AR7W section, Brendan DeTracey and C. K. Wang for assistance in the analysis of meteorological and hydrographic data, and Liam Petrie for making Fig. 1. We also thank Ken Drinkwater, John Lazier, and Peter Smith for their helpful comments on an early version of the manuscript. Helpful comments and suggestions were received from two anonymous reviewers. The TOPEX/Poseidon data were obtained from the NASA Pathfinder Project and PODAAC at JPL. This work was supported by the Canadian Panel for Energy Research and Development.

REFERENCES

- Benada, R., 1997: Merged GDR (TOPEX/Poseidon) users handbook. JPL D-11007, Jet Propulsion Laboratory, Pasadena, CA, 124 pp.
- Clarke, R. A., 1984: Transport through the Cape Farewell–Flemish Cap section. *Rapp. P. V. Reun. Cons. Int. Explor. Mer*, **185**, 120–130.
- , and J. C. Gascard, 1983: The formation of Labrador Sea water. Part I: Large-scale processes. *J. Phys. Oceanogr.*, **13**, 1764–1778.
- Colbourne, E., S. Narayanan, and S. Prinsenbergh, 1994: Climatic changes and environmental conditions in the Northwest Atlantic, 1970–1993. *ICES Mar. Sci. Symp.*, **198**, 311–322.
- Deser, C., and M. L. Blackmon, 1993: Surface climate variations over the North Atlantic Ocean during winter, 1900–1989. *J. Phys. Oceanogr.*, **23**, 1743–1753.
- DeTracey, B. M., and C. L. Tang, 1997: *Monthly Climatological Atlas of Surface Atmospheric Conditions of the Northwest Atlantic*. Vol. 152, *Canadian Data Report of Hydrography and Ocean Sciences*, 63 pp.
- Drinkwater, K. F., 1996: Atmospheric and oceanic variability in the Northwest Atlantic during the 1980s and early 1990s. *J. Northwest Atl. Fish. Sci.*, **18**, 77–97.
- Fofonoff, N. P., 1962: Dynamics of ocean currents. *The Sea*. Vol. 1: *Physical Oceanography*, Wiley-Interscience, 323–395.
- Greatbatch, R. J., and A. Goulding, 1989: Seasonal variations in a linear barotropic model of the North Atlantic driven by the Hellerman and Rosenstein wind stress field. *J. Phys. Oceanogr.*, **19**, 572–595.
- Han, G., and M. Ikeda, 1996: Basin-scale variability in the Labrador Sea from TOPEX/Poseidon and Geosat altimeter data. *J. Geophys. Res.*, **101**, 28 325–28 334.
- , and C. L. Tang, 1998: Circulation and transport in the western Labrador Sea from altimetry and hydrography. *Extended Abstracts, 1998 WOCE Conf.*, Halifax, NS, Canada, The Wace International Project Office, 199 pp.
- , and —, 1999: Velocity and transport in the Labrador Current determined from altimetric, hydrographic and wind data. *J. Geophys. Res.*, **104**, 18 047–18 057.
- Kalnay, E., and Coauthors, 1996: The NCEP/NCAR 40-Year Reanalysis Project. *Bull. Amer. Meteor. Soc.*, **77**, 437–471.

- Lazier, J. R. N., 1973: The renewal of Labrador Sea water. *Deep-Sea Res.*, **20**, 341–353.
- , and D. G. Wright, 1993: Annual velocity variations in the Labrador Current. *J. Phys. Oceanogr.*, **23**, 659–678.
- LeBlond, P. H., T. R. Osborn, D. O. Hodgins, R. Goodman, and M. Metge, 1981: Surface circulation in the western Labrador Sea. *Deep-Sea Res.*, **28A**, 683–693.
- Myers, R. A., J. Helbig, and D. Holland, 1989: Seasonal and interannual variability of the Labrador Current and west Greenland Current. ICES CM1989/C:16, 18 pp.
- Mysak, L. A., R. G. Ingram, J. Wang, and A. van der Baaren, 1996: The anomalous sea-ice extent in Hudson Bay, Baffin Bay and the Labrador Sea during three simultaneous NAO and ENSO episodes. *Atmos.–Ocean*, **34**, 313–343.
- Rapp, R. H., Y. M. Wang, and N. K. Pavlis, 1991: The Ohio State 1991 geopotential and sea surface topography harmonic coefficient models. Report 410, Dept. of Geodetic Science and Survey, The Ohio State University, Columbus, OH, 91 pp.
- Reynaud, T. H., A. J. Weaver, and R. J. Greatbatch, 1995: Summer mean circulation of the northwestern Atlantic Ocean. *J. Geophys. Res.*, **100**, 779–816.
- Smith, E. H., F. M. Soule, and O. Mosby, 1937: The Marion and General Green expeditions to Davis Strait and Labrador Sea. *Bull. U.S. Coast Guard*, Vol. 19, 259 pp.
- Tang, C. L., Q. Gui, and I. K. Peterson, 1996: Modeling the mean circulation of the Labrador Sea and the adjacent shelves. *J. Phys. Oceanogr.*, **26**, 1989–2010.
- , —, and B. M. DeTracey, 1999: A modeling study of upper ocean winter processes in the Labrador Sea. *J. Geophys. Res.*, **104**, 23 411–23 425.
- Thompson, K. R., J. R. N. Lazier, and B. Taylor, 1986: Wind-forced changes in Labrador Current transport. *J. Geophys. Res.*, **91**, 14 261–14 268.
- Veronneau, M., 1995: The GSD95 geoid model for Canada. Internal Report of Geodetic Survey Division, Department of Natural Resources, Ottawa, 11 pp.